An inhibitor of endothelial ETS transcription factors promotes physiologic and therapeutic vessel regression

Christopher M. Schafer[a], Jami M. Gurley[b,c], Katarzyna Kurylowicz[a], Prisca K. Lin[d], Wen Chen[b,c], Michael H. Elliott[b,c], George E. Davis[d], Faizah Bhatti[b,c,e], and Courtney T. Griffin[a,f,1]

[a]Cardiovascular Biology Research Program, Oklahoma Medical Research Foundation, Oklahoma City, OK 73104; [b]Department of Ophthalmology, University of Oklahoma Health Sciences Center, Oklahoma City, OK 73104; [c]Dean McGee Eye Institute, Oklahoma City, OK 73104; [d]Department of Molecular Pharmacology and Physiology, Morsani College of Medicine, University of South Florida School of Medicine, Tampa, FL 33612; [e]Neonatal Perinatal Medicine, Department of Pediatrics, University of Oklahoma Health Sciences Center, Oklahoma City, OK 73104; and [f]Department of Cell Biology, University of Oklahoma Health Sciences Center, Oklahoma City, OK 73104

Edited by Jeremy Nathans, Johns Hopkins University School of Medicine, Baltimore, MD, and approved September 8, 2020 (received for review July 28, 2020)

During the progression of ocular diseases such as retinopathy of prematurity and diabetic retinopathy, overgrowth of retinal blood vessels results in the formation of pathological neovascular tufts that impair vision. Current therapeutic options for treating these diseases include antiangiogenic strategies that can lead to the undesirable inhibition of normal vascular development. Therefore, strategies that eliminate pathological neovascular tufts while sparing normal blood vessels are needed. In this study we exploited the hyaloid vascular network in murine eyes, which naturally undergoes regression after birth, to gain mechanistic insights that could be therapeutically adapted for driving neovessel regression in ocular diseases. We found that endothelial cells of regressing hyaloid vessels underwent down-regulation of two structurally related E-26 transformation-specific (ETS) transcription factors, ETS-related gene (ERG) and Friend leukemia integration 1 (FLI1), prior to apoptosis. Moreover, the small molecule YK-4-279, which inhibits the transcriptional and biological activity of ETS factors, enhanced hyaloid regression in vivo and drove Human Umbilical Vein Endothelial Cells (HUVEC) tube regression and apoptosis in vitro. Importantly, exposure of HUVECs to sheer stress inhibited YK-4-279–induced apoptosis, indicating that low-flow vessels may be uniquely susceptible to YK-4-279–mediated regression. We tested this hypothesis by administering YK-4-279 to mice in an oxygen-induced retinopathy model that generates disorganized and poorly perfused neovascular tufts that mimic human ocular diseases. YK-4-279 treatment significantly reduced neovascular tufts while sparing healthy retinal vessels, thereby demonstrating the therapeutic potential of this inhibitor.

ERG | FLI1 | hyaloid vessels | oxygen-induced retinopathy | YK-4-279

Ocular blood vessels are regulated so as to balance the high nutritional demands of the retina against the impairment of visual function that results from hypervascularization (1). In diseases such as retinopathy of prematurity (ROP) and diabetic retinopathy (DR), this balance is lost and results in the formation of neovascular (NV) tufts originating from the superficial retinal vascular layer which physically impede the transmission of light (2–4). Moreover, retinal neovessels are inherently unstable and prone to hemorrhage, which then elevates ocular inflammation and further exacerbates visual dysfunction (5, 6). Because of this, ROP and DR are among the leading causes of blindness in infants and adults, respectively (7, 8).

Vascular endothelial growth factor (VEGF) has long been recognized as an important proangiogenic signaling molecule, and it is well established that VEGF plays a role in the progression of NV disease (9, 10). For this reason, many current therapeutic treatments suppress VEGF signaling to reduce the extent of ocular vascular overgrowth (11–14). However, VEGF plays an essential role in many developmental processes (15), raising concerns regarding the long-term consequences of VEGF inhibition, particularly in infants with ROP (16). For example, one study demonstrated a reduction in systemic VEGF for up to 2 mo after intravitreal anti-VEGF treatment (17). Moreover, in longitudinal studies anti-VEGF treatments have shown a tendency for reactivation of NV complications after treatment is suspended (18, 19) and an association with long-term abnormalities in retinal vascular structure and ocular function (20–22). These adverse consequences may be overcome by targeted treatment options optimized for the removal of pathological neovessels.

Intriguingly, certain ocular blood vessel networks naturally regress during development of the eye. The underlying mechanisms of these regression processes may therefore inform innovative therapeutic approaches aimed at the promotion of NV tuft regression in diseases such as ROP and DR. One well-documented example of physiological vascular regression occurs with the hyaloid vessels, which extend from the optic nerve head through the vitreous and wrap around the lens to nourish the developing anterior segment of the eye. Shortly after birth in mice (and at midgestation in humans), the hyaloid vessels initiate a regression process culminating in their complete elimination within 2 to 3 wk (23). Failed execution of this process results in a condition called persistent hyperplastic vitreous, in which the remaining hyaloid vessels impair visual function similarly to retinal neovessels found in NV disorders (24).

Significance

Premature babies and diabetic patients can become blind when too many blood vessels develop in their eyes, and therapeutic strategies are needed for eliminating those extra vessels. We studied newborn mice that naturally undergo loss of some eye vessels to identify ways to promote blood vessel regression and elimination. We identified a class of proteins called E-26 transformation-specific transcription factors that are down-regulated during normal vessel regression, especially in vessels with slow blood flow. Importantly, we found that a drug that disables these proteins can be used in mouse eyes to eliminate abnormal, slow-flow blood vessels similar to those seen in premature babies and diabetic patients.

Author contributions: C.M.S., G.E.D., and C.T.G. designed research; C.M.S., J.M.G., K.K., P.K.L., and W.C. performed research; C.M.S., J.M.G., K.K., P.K.L., W.C., M.H.E., G.E.D., F.B., and C.T.G. analyzed data; and C.M.S. and C.T.G. wrote the paper.

The authors declare no competing interest.

This article is a PNAS Direct Submission.

Published under the PNAS license.

[1]To whom correspondence may be addressed. Email: courtney-griffin@omrf.org.

This article contains supporting information online at https://www.pnas.org/lookup/suppl/doi:10.1073/pnas.2015980117/-/DCSupplemental.

First published October 5, 2020.

Downloaded at Palestinian Territory, occupied on December 11, 2021

www.manaraa.com

Hyaloid vessel regression is dependent on macrophages, which initiate regression via the production of Wnt7b that induces apoptosis of vascular endothelial cells (ECs) (25–27). However, the broad expression pattern of Wnt7b (28) and its proangiogenic function in other contexts (29, 30) suggest that additional factors are necessary for the induction of hyaloid regression. For example, local VEGF concentrations (31), decreased blood flow (32), Angiopoietin-2 (33), and inflammatory cytokines (34) all influence hyaloid regression either directly or indirectly. Therefore, hyaloid regression results from the integration of many external cues, which likely prevent improper execution of a costly and irreversible vascular fate decision.

In this study, we sought to define mechanistic aspects of hyaloid vessel regression, reasoning that downstream vascular effectors of this physiologic process may yield viable proregressive therapeutic targets. We identified two E-26 transformation-specific (ETS) family transcription factors that were strikingly down-regulated in regressing hyaloid vessel endothelial cells. Utilization of a small molecule with the capacity to inhibit this class of transcription factors resulted in the induction of vascular regression in vivo and in vitro. Moreover, inhibitor treatment significantly resolved vascular abnormalities in a murine oxygen-induced retinopathy (OIR) model of ROP, demonstrating the therapeutic potential of targeting vascular ETS family transcription factors to promote regression of pathological ocular blood vessels.

Results

Coordinated Constriction and Apoptosis of Hyaloid Vessels Excludes Blood Flow from Actively Regressing Vessels. In order to investigate factors playing a role in physiological blood vessel regression, murine hyaloids were dissected and imaged by flat mount as previously described (26), demonstrating ∼50% fewer vessels between postnatal day 4 (P4) and P8 (Fig. 1*A* and *SI Appendix*, Fig. S1*A*). Hyaloid vessel regression results from the apoptosis of ECs that line vascular luminal surfaces (35, 36), which we visualized by terminal deoxynucleotidyl transferase dUTP nick end labeling (TUNEL) (Fig. 1*B*). From P4 to P8 the percentage of TUNEL$^+$ hyaloid vessels increased from ∼5 to ∼25% (*SI Appendix*, Fig. S1*B*), indicating that this is a useful experimental window in which to study vascular regression due to the presence of vessels at various stages of regression.

TUNEL staining revealed a unique pattern in which dying cells were primarily clustered on distinct vascular branches (Fig. 1*B*). We observed the same staining pattern for active caspase-3, a more specific marker of the apoptotic cell death pathway (*SI Appendix*, Fig. S1*C*). Meeson et al. previously suggested that the segmental nature of hyaloid vessel apoptosis indicates the presence of a coordinating factor, such as blood flow, that synchronizes EC death within a particular vascular branch (32). In support of this model, we determined that at both P4 and P8 the diameters of apoptotic vessel branches were significantly reduced compared to their nonapoptotic counterparts (Fig. 1*C*). In fact, from P4 to P8 there was a general reduction in the diameters of nonapoptotic vessels (from ∼15 to ∼10 μm), whereas apoptotic vessel diameters remained constant at ∼5 to 6 μm (Fig. 1*C*). Furthermore, immunostaining for the red blood cell (RBC) marker Ter119 demonstrated the exclusion of RBCs from constricted, regressing vessels (Fig. 1*D*). These data support published evidence of a correlation between the constriction and apoptosis of hyaloid vessels (32), altogether suggesting that the cessation of blood flow is an important factor regulating hyaloid vessel regression.

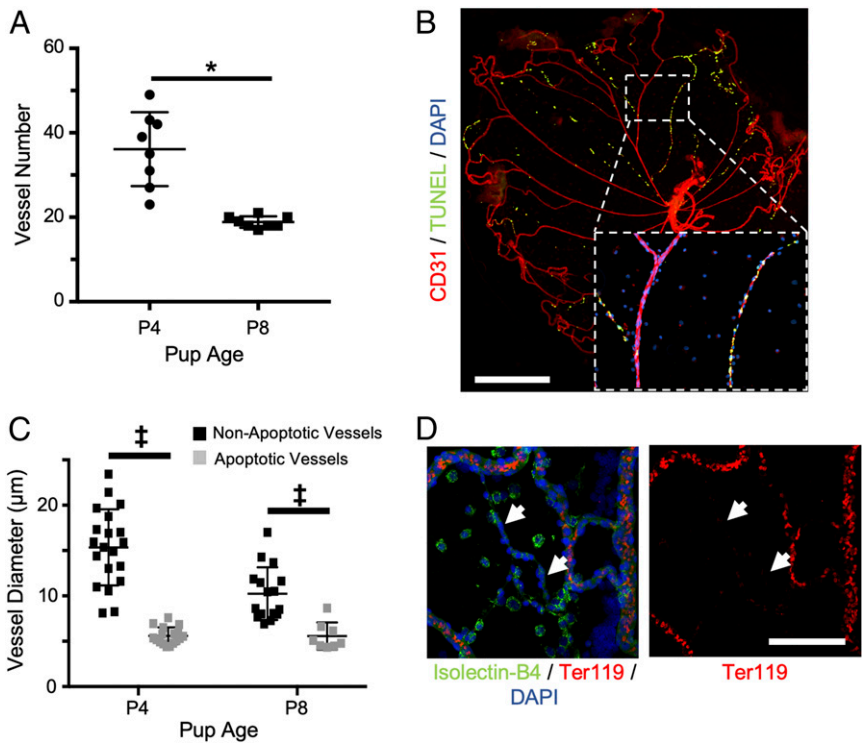

Fig. 1. Segmental apoptosis of constricted vessels is observed during hyaloid regression. (*A*) Hyaloid vessel regression ($n = 8$) was quantified by counting the number of vessels crossing a line drawn at 50% of the total diameter of hyaloid flat mounts (*SI Appendix*, Fig. S1*A*). (*B*) Hyaloid vessel flat mount from a wild-type P8 mouse stained for TUNEL (green) and CD31 (red). (*Inset*) Magnified view of boxed region demonstrating the coordination of apoptosis in distinct vascular branches. (Scale bar, 500 μm.) (*C*) Quantification of vessel diameters for nonapoptotic ($n = 12$ to 20) and apoptotic vessels ($n = 8$ to 15) from P4 and P8 wild-type mice. (*D*) Hyaloid vessels from a P6 wild-type mouse were immunostained for Isolectin-B4 (green) and Ter119 (red) to visualize the exclusion of red blood cells from constricted hyaloid vessels (white arrows). (Scale bar, 100 μm.) For *B* and *D*, nuclei were counterstained with DAPI (blue). *$P < 0.05$ (two-tailed Student's *t* test). ‡$P < 0.05$ (two-way ANOVA). Error bars: SD.

PHYSIOLOGY
Downloaded at Palestinian Territory, occupied on December 11, 2021
www.manaraa.com

ETS-Related Gene Is Down-Regulated in Constricted Regressing Hyaloid Vessels. ETS-related gene (ERG) is an EC-specific ETS family transcription factor that has been reported to promote vascular regression when genetically deleted in mice (37). We used immunofluorescence to compare the expression of ERG in hyaloid vessels at various stages of regression and observed a notable absence of ERG from highly constricted vessels (Fig. 2*A*). Moreover, ERG down-regulation was observed in constricted vessels that were not yet TUNEL$^+$ (Fig. 2*B*, white arrow). Some ECs on TUNEL$^+$-constricted vessels appeared to maintain ERG expression, although the staining pattern was notably irregular and largely excluded from the nucleus (yellow arrow in Fig. 2*B*) when compared to adjacent nonconstricted vessels. Together, these data raise the possibility that the down-regulation and/or nuclear exclusion of ERG may play a transcriptional role in promoting vessel regression. Indeed, it has been reported that inhibition of ERG results in EC apoptosis due to transcriptional down-regulation of the ERG target gene *Cdh5*, which encodes the adhesion molecule vascular endothelial (VE)-cadherin (38). Intriguingly, we observed down-regulation of VE-cadherin along with ERG in constricted hyaloid vessels (*SI Appendix*, Fig. S2), suggesting that a similar mechanism may function during hyaloid regression.

In both mice and humans, regression of the hyaloid vessels within the vitreous coincides with robust angiogenesis of ECs located on the superficial retinal surface that faces the vitreous (39). The spatiotemporal proximity of these vessel networks therefore stands in contrast to their opposing vascular fates. We used immunofluorescence to compare expression of ERG within these two EC populations in cross-sections of eyes from P8 wild-type mice. Whereas angiogenic retinal ECs were marked by robust ERG expression, regressive hyaloid ECs showed little ERG expression, suggesting that ERG down-regulation may play a role in distinguishing the behavior of these two vessel networks (Fig. 2*C*).

A Pharmacological Inhibitor of ETS Transcription Factors Promotes Vessel Regression In Vivo and In Vitro. To assess the role of ERG in hyaloid vessel regression, we intravitreally administered YK-4-279, a small molecule with the capacity to inhibit the transcriptional and biological activity of ERG (*SI Appendix*, Fig. S3*A*) (40) to P5 pups and counted hyaloid vessel numbers at P7. Compared to vehicle-injected littermate controls, YK-4-279 injection resulted in an ∼40% reduction in hyaloid vessel number, which is consistent with a proregressive effect on the hyaloid vasculature (Fig. 3 *A* and *B*).

In addition to ERG, YK-4-279 likewise inhibits other ETS transcription factors, including the structurally related transcription factor Friend Leukemia Integration 1 (FLI1) (40–42), which is 62% identical and 73% similar to ERG (*SI Appendix*, Fig. S3*B*). As with ERG, we observed a reduction in endogenous FLI1 expression in constricted hyaloid vessels (Fig. 3*C*). Some ECs on those constricted vessels appeared to maintain FLI1 expression, although the nuclear staining pattern was notably irregular when compared to adjacent vessels (white arrow in Fig. 3*C*), as described above for ERG. ERG and FLI1 have previously been shown to regulate overlapping gene sets and to compensate transcriptionally for one another, suggesting that the proregressive effects of YK-4-279 might result from the inhibition of both ERG and FLI1 (43–45). To test this possibility, we quantified hyaloid vessel regression in mice following genetic deletion of *Erg* in ECs. We crossed Erg^{flox} mice to the tamoxifen-inducible endothelial *Cdh5(PAC)-Cre*^{ERT2} line to generate $Erg^{fl/fl}$;*Cdh5(PAC)-Cre*^{ERT2} (Erg^{iECko}) mice and administered tamoxifen by oral gavage at P3, P4, and P5 to delete *Erg* in ECs. Despite efficient *Erg* deletion (*SI Appendix*, Fig. S3*C*), we observed no differences in hyaloid vessel number between Erg^{iECko} mice and their littermate controls at P7 (*SI Appendix*, Fig. S3*D*). Therefore, the proregressive effects of YK-4-279 likely result from the broader inhibition of ETS family transcription factors in hyaloid vessels, rather than from the specific inhibition of ERG.

To further characterize its proregressive potential, YK-4-279 was added to preestablished three-dimensional (3D) cultures of Human Umbilical Vein Endothelial Cells (HUVECs). Importantly, this culture model recapitulates many aspects of in vivo vessel morphology, including the formation of vascular lumens, and has previously been used to model vascular regression (34). Treatment with YK-4-279 resulted in a significant, dose-dependent loss of vascular luminal area at concentrations ≥2.5 μmol/L (Fig. 3 *D* and *E*), decreased procaspase-3 stain (indicative of apoptosis; *SI Appendix*, Fig. S4*A*) and enhanced the proregressive effects of inflammatory cytokines that we previously demonstrated play a role in hyaloid regression (*SI Appendix*, Fig. S4*B*) (34). Taken together, these data demonstrate a proregressive function of YK-4-279 in vitro, complementing our in vivo observations.

YK-4-279 Promotes Flow-Dependent Vascular Regression In Vitro. Despite the formation of vascular lumens, HUVECS grown in

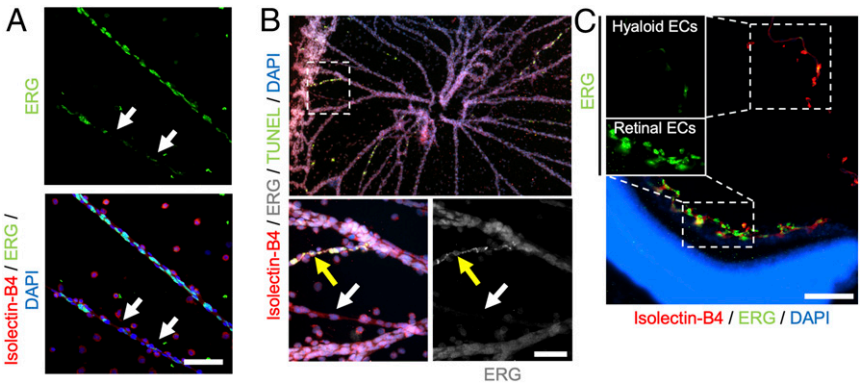

Fig. 2. The transcription factor ERG is down-regulated in constricted hyaloid vessels. (*A*) Flat-mount hyaloid vessels from a P6 wild-type mouse immunostained for Isolectin-B4 (red) and ERG (green). Arrows indicate a constricted hyaloid vessel with reduced nuclear ERG expression. (Scale bar, 100 μm.) (*B*, *Top*) Flat-mount hyaloid vessels from a P8 wild-type mouse immunostained for Isolectin-B4 (red), ERG (gray), and TUNEL (green). (*B*, *Bottom*) Magnified views of region outlined in white. The white arrow demonstrates down-regulation of ERG in a constricted hyaloid vessel that is not yet TUNEL$^+$. The yellow arrow indicates a highly constricted, apoptotic vessel with irregular, nonnuclear ERG expression. (Scale bar, 50 μm.) (*C*) Immunostained cross-section of an eye from a P8 wild-type mouse allowing comparison of ERG expression (green) between retinal and hyaloid ECs that are stained with Isolectin-B4 (red); nuclei are counterstained with DAPI (blue). (*Insets*) The solo ERG channel for hyaloid (*Top*) and retinal (*Bottom*) ECs demonstrates the absence of ERG expression in regressing hyaloid ECs. (Scale bar, 50 μm.)

Downloaded at Palestinian Territory, occupied on December 11, 2021
www.manaraa.com

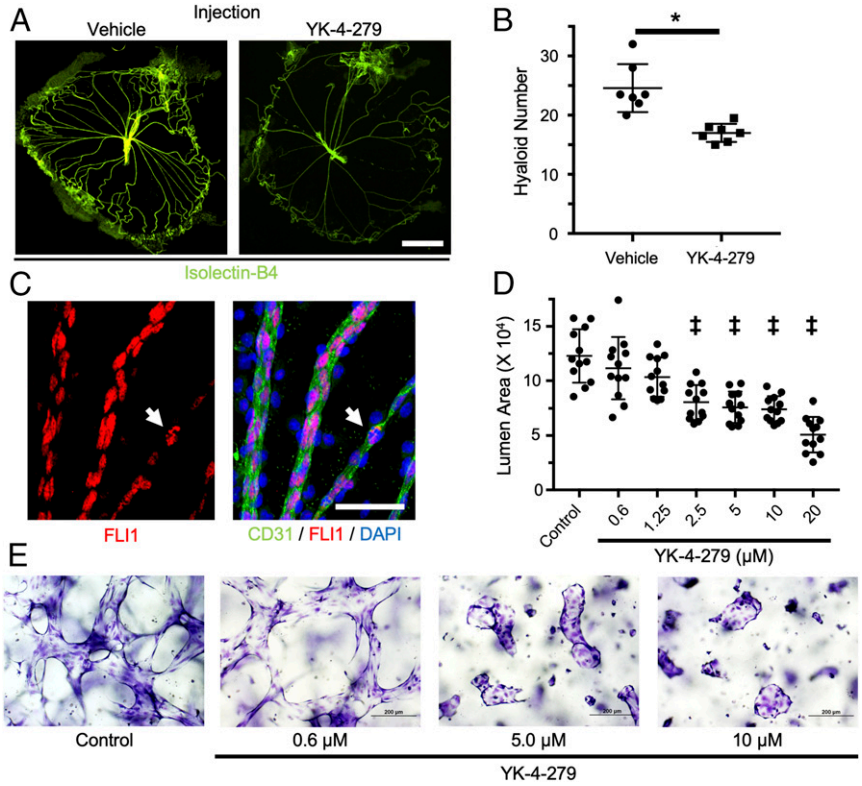

Fig. 3. YK-4-279, a pharmacological inhibitor of ETS factors, promotes vascular regression in vivo and in vitro. (*A*) Representative flat-mount images of hyaloid vessels from P7 wild-type mice administered an intravitreal injection of vehicle or YK-4-279 at P5. Hyaloids were stained with Isolectin-B4 (green). (Scale bar, 500 μm.) (*B*) Quantification of regression in hyaloids ($n = 7$) treated with vehicle or YK-4-279 as in *A*. (*C*) Flat-mount hyaloid vessels from a P7 wild-type mouse were immunostained for CD31 (green) and FLI1 (red). As observed for ERG, FLI1 expression is mostly reduced in constricted hyaloid vessels compared to nearby hyaloid vessels with a wider diameter. Some ECs in constricted vessels still express FLI1 (arrow), although its staining pattern is irregular compared to the pan-nuclear staining pattern seen in adjacent vessels. (Scale bar, 50 μM.) (*D*) Quantification of average lumen area in 3D HUVEC cultures ($n = 12$) treated with the indicated concentrations of YK-4-279 for 48 h. (*E*) Representative images of 3D HUVECs stained with toluidine blue demonstrating the effects of YK-4-279 on luminal area. $^{*}P < 0.05$ (two-tailed Student's *t* test). $^{‡}P < 0.05$ (one-way ANOVA). Error bars: SD.

this 3D culture model lack the blood flow that would be present in vivo. The substantial proregressive effects of YK-4-279 in this model, taken together with the specificity of in vivo regression to constricted hyaloid vessels, raises the possibility that the absence of blood flow is an important prerequisite for YK-4-279–induced vascular regression. This possibility is supported by a recent report that the transcriptional consequences of ERG inhibition are greatly mitigated in ECs exposed to sheer stress (46). To test the effect of flow on YK-4-279–mediated vessel regression, we treated HUVECs with YK-4-279 in an Ibidi flow chamber system. HUVECs were plated on Luer$^{0.6}$ flow cells at 80 to 90% confluence and were equilibrated under static or flow (10 dyn/cm^2) conditions for 24 h to mimic flow conditions expected for small caliber vessels such as the hyaloids (47). Following equilibration, 5 μmol/L YK-4-279 (or a vehicle control) was added to the media, and HUVECs were maintained under their respective flow conditions for an additional 24 h. Under static conditions, YK-4-279 treatment resulted in significantly reduced cell numbers and increased active caspase-3 staining (Fig. 4 *A* and *B*), indicating an increase in EC apoptosis. In contrast, under flow conditions YK-4-279 treatment had no apparent effect on cell number or on active caspase-3 staining (Fig. 4 *A* and *B*), demonstrating a protective effect of flow on YK-4-279–mediated EC death in vitro. Interestingly, YK-4-279 treatment inhibited the alignment of HUVECs to flow, resulting in a more cobblestone shape under flow conditions when compared to vehicle-treated cells (Fig. 4*C*). Therefore, YK-4-279 mediated effects on EC behavior but failed to drive EC death under in vitro flow conditions.

YK-4-279 Induces Regression of Retinal Neovessels following Oxygen-Induced Retinopathy. OIR has been established as a useful in vivo model of ROP that recapitulates the NV component of both ROP and DR (48, 49). Briefly, P7 wild-type mice are transferred to hyperoxic conditions (75% O_2) for 5 d, which results in vaso-obliteration of the central retina. At P12, mice are returned to room air (21% O_2), which results in hypoxia-induced retinal neovascularization that peaks at P17 to P18. Importantly, due to their tortuous and disorganized structure, retinal neovessels are poorly perfused relative to healthy retinal vessels (50, 51), suggesting that they may be uniquely susceptible to YK-4-279–induced regression.

To test this possibility, P17.5 mice that had been subjected to the OIR protocol were given intravitreal injections of YK-4-279 in one eye and a vehicle control in their contralateral eye. Two days after injection, P19.5 mice were euthanized, and retinas were dissected and immunostained for CD31 to quantify the retinal NV area as previously described (48). YK-4-279 injection resulted in a decrease in retinal NV area in 9 of 11 mice, with only one mouse showing an increase in neovessels in the inhibitor-injected eye relative to the control eye. Altogether, we observed a significant ~40% reduction in retinal NV area with inhibitor treatment (Fig. 5 *A* and *B*). Importantly, healthy perfused retinal vessels located in the peripheral retina appeared to be spared from YK-4-279–induced regression (Fig. 5*A*), consistent with a protective effect of blood flow. Likewise, when we administered YK-4-279 to wild-type adult mice with normal retinal vasculature, we observed no effects of the inhibitor on either total vascular area or branch points (52)

Downloaded at Palestinian Territory, occupied on December 11, 2021

www.manaraa.com

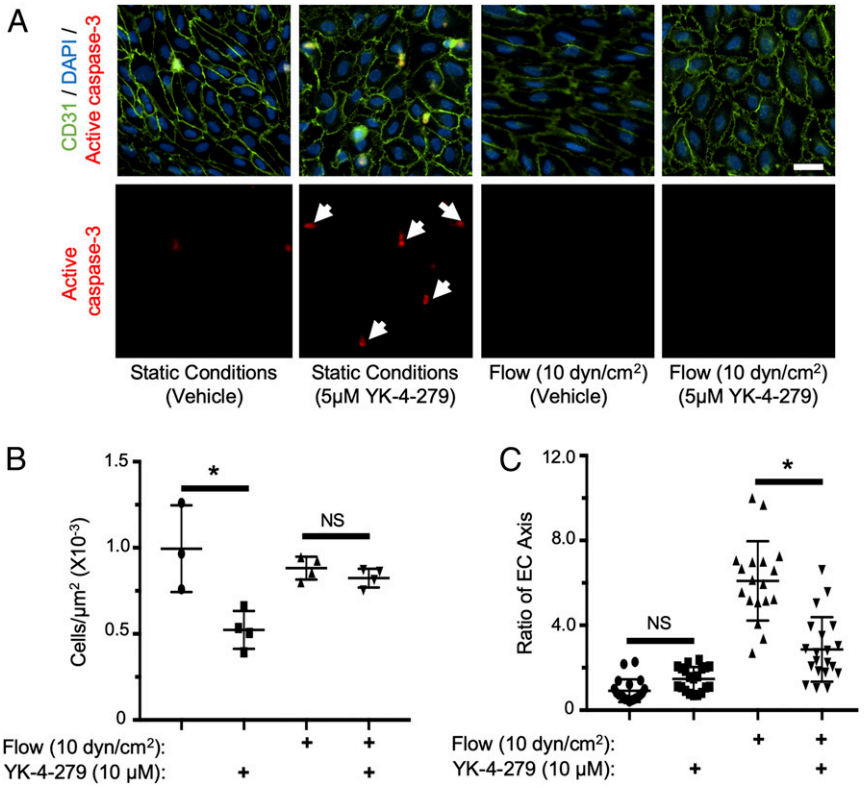

Fig. 4. YK-4-279 induces flow-dependent HUVEC apoptosis in vitro. (*A*) Images of HUVECs stained for CD31 (green) and active caspase-3 (red) under the indicated flow and YK-4-279 treatment conditions; nuclei were counterstained with DAPI (blue). White arrows indicate apoptotic cells (active caspase-3$^+$) detected after YK-4-279 treatment under static but not under flow (10 dyn/cm^2) conditions. (Scale bar, 30 μm.) (*B*) Quantification of cells/μm^2 ($n = 3$ to 4) using experimental conditions in *A*. (*C*) Quantification of HUVEC morphology ($n = 18$) as measured by the EC axis parallel to flow relative to the axis perpendicular to flow. *$P < 0.05$ (two-tailed Student's *t* test). NS = not significant. Error bars: SD.

(*SI Appendix*, Fig. S5 *A–C*). Surprisingly, along with the reduction in NV area in the OIR model, we observed ∼60% less retinal avascular area following YK-4-279 treatment (Fig. 5 *A* and *C*), which suggests that inhibitor treatment may facilitate normal revascularization of the retina after regression of NV tufts.

Discussion

Cardiovascular function requires complex, organ-specific vascular patterning achieved through the continuous integration of pro- and antigrowth signals. This has led to the recognition of well-established angiogenic pathways that coordinate vascular development and maintenance. By contrast, little is known about molecular pathways that promote the regression of preexisting vessels (53). This is partly due to the paucity of naturally occurring examples of vascular regression. Indeed, much of the literature devoted to the subject refers to the pruning of dispensable vessels during vessel network maturation (54). However, this is often a nonapoptotic (55, 56) process limited to a small percentage of cells within a vessel network and is therefore not associated with substantial changes in tissue vascularization.

A small number of physiological regression processes have been documented in which the complete involution of a pre-established, functional vascular network is brought about over a short period of time. Among these are luteolysis in the adult ovarian cycle (57) and the developmental regression of a small number of ocular blood supplies, including the hyaloid vessels (23). Although rare, regression of this form is uniquely poised to offer insights into the therapeutic induction of vascular regression in cases of pathological hypervascularization. The eye appears to be particularly susceptible to hypervascularization, as evidenced by a number of ocular pathologies with well-documented vascular abnormalities, including ROP and DR (2, 4). This susceptibility may reflect the delicate balance required for satisfying the high nutritional demands of the retina against the physical impediment that blood vessels impose on light transmission. The hyaloids are therefore a unique and experimentally tractable system in which to identify pro-regressive molecular pathways relevant to the treatment of ocular NV diseases.

To date, studies of factors that contribute to hyaloid regression have identified proregressive cues linked to Wnt ligands (26), Angiopoietin-2 (58), proinflammatory cytokines and thrombin (34), VEGF depletion (36), and blood flow cessation (32). However, many of these stimuli also play important functions in non-regressive contexts, suggesting that few external stimuli are by themselves sufficient for the initiation of regression. Our observation that the ECs of regressive hyaloid vessels are marked by the loss of nuclear ERG/FLI1 expression demonstrates an endothelial phenotype associated with vascular regression. ERG/FLI1 are highly expressed by ECs, where they regulate many endothelial genes (37, 59). Embryonic deletion of *Erg* is lethal, although its postnatal deletion is associated with more subtle phenotypes (60). One likely explanation for this temporal difference in phenotypic severity is the acquisition of functional redundancy with other endothelial ETS family transcription factors, such as FLI1, with which ERG shares structure, endothelial expression, and many target genes (43, 44).

Several ETS family transcription factors, including ERG and FLI1, can become misregulated in nonendothelial cells due to chromosomal translocation events and thereby contribute to various cancers, including prostate carcinoma and Ewing sarcoma (61, 62). For this reason, inhibitors such as YK-4-279, which target the biological activity of ETS factors, have been developed for

Downloaded at Palestinian Territory, occupied on December 11, 2021
www.manaraa.com

therapeutic applications (63–66). However, the impact of these inhibitors on ECs, which express at least seven endogenous ETS factors (ETS1/2, ETV2/6, ERG, FLI1, and ELK3) (67), has not been explored. Our studies now demonstrate the capacity of YK-4-279 to modulate vascular behavior in vitro and in vivo. YK-4-279 was originally characterized for its ability to block the pro-oncogenic interaction between the Ewing sarcoma fusion protein EWS-FLI1 and RNA-helicase A (63). YK-4-279 was subsequently shown to inhibit ERG-mediated transcription in COS7 cells and to diminish ERG and ETV1 target gene transcripts in prostate cancer cell lines (40). Our data indicate that YK-4-279 can inhibit binding of both ERG and RNA Polymerase II to the promoter of the ERG target gene *Cdh5* in HUVECs (*SI Appendix*, Fig. S3*A*). Because ERG and FLI1 share >96% sequence identity in their DNA-binding domains (*SI Appendix*, Fig. S3*B*), we predict that YK-4-279 can similarly inhibit the DNA-binding and transcriptional capacity of FLI1 in ECs. However, since ETS factors like ERG and FLI1 bind to the same DNA motif and can regulate the transcription of many genes (59), it will be challenging to determine which specific gene target(s) mediate the proregressive effects of YK-4-279. One possibility is that regression proceeds through the down-regulation of VE-Cadherin, as has been reported previously (38) and was here observed in vivo. In addition, ERG/FLI1 transcriptionally regulate other prosurvival pathways that play roles in vessel stability (68, 69). Therefore, it seems likely that complex transcriptional effects account for the proregressive potential of YK-4-279. Altogether, we acknowledge that the precise targets of YK-4-279 in ECs and the mechanisms by which it promotes vascular regression will require further investigation.

It is presently unclear what initiates ERG/FLI1 down-regulation in regressing hyaloids. ERG is robustly expressed in most endothelial populations (for which reason it is commonly employed as an EC nuclear marker) and has been observed to be down-regulated only under specific conditions (43, 70). One of these studies reported transcriptional repression of ERG in vitro by inflammatory cytokines (70). We have recently demonstrated a proregressive role of inflammatory cytokines in hyaloid regression (34), so it is interesting to speculate that such factors might contribute to the down-regulation of ERG in regressing hyaloids, although this will require further studies. In addition, the apparent coordination of ERG/FLI1 down-regulation along constricted hyaloid vessels suggests flow-dependent regulation, but we and others have failed to observe this effect in vitro (46). We therefore suggest that the loss of blood flow and down-regulation of ERG/FLI1 are independent events, thereby providing a multifactor check against unwanted regressive events that are costly and irreversible. Moreover, ensuring a lack of blood flow prior to the onset of regression likely prevents intraocular hemorrhage at sites of EC apoptosis. Interestingly, Peghaire et al. recently reported that the transcriptional consequences of ERG inhibition in hepatic ECs were eliminated by exposure to high sheer stress (20 dyn/cm^2) (46). Therefore, we hypothesize a similar mechanism functions in the eye as a check against the death of ECs in perfused vessels with down-regulated ERG/FLI1. Nevertheless, further investigation into the mechanistic causes of capillary constriction and ERG/FLI down-regulation during hyaloid regression are warranted.

The specificity of YK-4-279–induced regression to low sheer stress conditions affords a unique opportunity for the treatment of ocular NV disorders. Due to their tortuous and disorganized structure, retinal neovessels are poorly perfused. We therefore hypothesized that these vessels, and not their healthy counterparts, would be uniquely susceptible to YK-4-279–induced regression. Indeed, YK-4-279 injection resulted in an improvement in retinal vascular structure in the OIR model. Administration of YK-4-279 resulted in a significant reduction in retinal NV tufts without any apparent effects on healthy vessels in the OIR model or in normal adult eyes, consistent with a model in which flow confers protection against the proregressive effects of the inhibitor, as we had seen in vitro.

Our observation that YK-4-279 treatment additionally resulted in a decreased retinal avascular area was surprising and highlights an additional potential benefit of this proregressive treatment over traditional antiangiogenic therapies, which sometimes result in an increased retinal avascular area (16, 22). Indeed, we found nearly complete vascularization of the central retina in ~60% of inhibitor-treated eyes by P20. If left untreated, OIR-induced neovessels spontaneously regress around P25, and the central retina is eventually revascularized in a normal pattern by the remaining ECs (48, 71). We therefore hypothesize that YK-4-279 facilitates normal retinal revascularization by expediting the clearance of pathological neovessels. Alternatively, we cannot yet rule out the possibility of direct stimulation of retinal vascularization by YK-4-279, which will be the focus of future studies.

Methods

Mice. Mice used in this study include C57BL/6J (The Jackson Laboratory; #000664), *Erg*^{flox} (gift of Joshua Wythe, Baylor College of Medicine; available through The Jackson Laboratory; #030988), and *Cdh5(PAC)-Cre*^{ERT2} (gift of Ralf Adams, Max Planck Institute for Molecular Biomedicine; available through Taconic; #13073), which have previously been described (72, 73). Mice used for hyaloid studies were maintained at the Oklahoma Medical Research Foundation animal facility; C67Bl/6J mice used for OIR studies were maintained at the Dean McGee Eye Institute animal facility. Both male and female mice were included in all studies. Genotyping of *Erg*^{flox} was performed using the primers 5′-GAGATGGCGCAACGCAATTAATG-3′, 5′-AGAGTCTCTGCACACAGAACTTCC-3′, and 5′-AATGCTCTGGTAAGGCACACAAGG-3′, which yielded 346- and 312-bp amplicons for *Erg*^{flox} and *Erg*$^{+}$, respectively. Genotyping of *Cdh5(PAC)-Cre*^{ERT2} mice was performed using the primers 5′-TCCTGATGGTGCCTATCCTC-3′ and 5′-CGAACCTGGTCGAAATCAGT-3′, which yielded a 473-bp amplicon. Tamoxifen-induced deletion of *Erg* in *Erg*$^{flox/flox}$*;Cdh5(PAC)-Cre*^{ERT2} mice was accomplished by oral gavage of 2 μL of 25 mg/mL tamoxifen (Sigma) dissolved in peanut oil, administered to pups at P3, P4, and P5.

Hyaloid Vessel Dissection and Quantification. Murine hyaloid vessels were dissected and quantified as described previously (26). Briefly, eyes were enucleated from P4 to P8 mice, fixed for 30 min in 4% paraformaldehyde, and transferred to phosphate-buffered saline (PBS) on ice. The cornea was removed, and the sclera and retinal pigmental epithelium were peeled away, leaving the retinal cup containing the lens loosely wrapped with the hyaloid vessels. The lens was then removed, and the hyaloids were carefully peeled away and transferred in a drop of PBS to a slide for flat-mount imaging. Blinded quantification of hyaloid regression was performed by counting the number and diameter of vessels crossing an outline drawn around flat mounts (labeled with Isolectin-B4 or CD31) that was reduced in size by 50% (Fig. 1*A*).

Immunofluorescence Imaging. Hyaloid vessel flat mounts were dried for 30 min at room temperature and then blocked/permeabilized by overnight incubation in 1% bovine serum albumin (BSA) and 0.5% Triton X-100 in PBS at 4 °C. Eye cross-sections were prepared by collecting 10-μm thick cryosections from P8 wild-type eyes embedded in optimal cutting temperature compound (Tissue-Tek). Sections were dried at room temperature for 30 min, washed with PBS, and then blocked and permeabilized as above. Primary antibodies were diluted in 1% BSA and then incubated with samples overnight at 4 °C. Primary antibodies used for immunostaining in this study include Isolectin-B4 (1:50, Invitrogen; #I21411), anti-CD31 (1:50, Fisher; #AF3268), anti-ERG (1:100, Abcam; #ab92513), anti-FLI1 (1:100, Abcam; #ab15289), anti-Ter119 (1:50, BioLegend; #116214), anti-VE Cadherin (1:50, BD Biosciences; #550548), and antiactive caspase-3 (1:100, Cell Signaling; #9661S). TUNEL staining was performed with the In Situ Cell Death Detection Kit (Sigma), following the manufacturer's guidelines. All imaging was performed on a Nikon Eclipse Ti-E epifluorescence microscope or a Nikon C2 confocal microscope and analyzed using NIS-Elements software.

Intravitreal Injection of YK-4-279 in Neonatal Mice. Hyperthermia-induced anesthesia of wild-type P5 mice was accomplished by submerging pups in ice for 5 to 8 min after placing them in a latex blanket wrapped in foil to avoid direct contact between the pup and ice. Once anesthetized (assessed by toe pinch), eyes were administered a drop of proparacaine hydrochloride

Downloaded at Palestinian Territory, occupied on December 11, 2021

www.manaraa.com

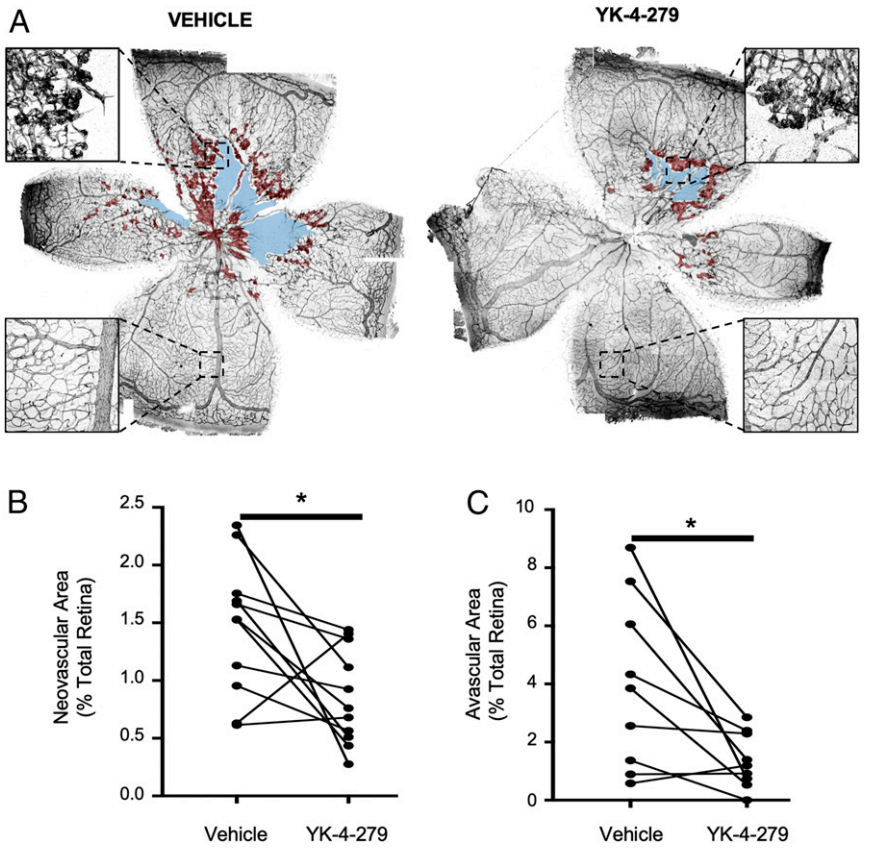

Fig. 5. YK-4-279 reduces neovascularization and avascular areas in mouse retinas following OIR. (*A*) Representative images of P19.5 retinas immunostained for CD31 (black) were stitched from 50 to 60 composite images using Nikon NIS-Elements software. Retinas shown are from an individual mouse that was subjected to the OIR protocol and then intravitreally injected with YK-4-279 or a vehicle control in contralateral eyes at P17.5. Retinal neovessels and avascular areas are shaded in red and blue, respectively. (*Insets*) Magnifications demonstrate centrally located retinal neovessels and peripheral healthy vessels. Retinal neovascular area (*B*) and avascular area (*C*) were quantified ($n = 9$) and compared between YK-4-279–injected and vehicle-injected eyes. Contralateral eyes from the same mouse are indicated by the lines connecting data points. *$P < 0.05$ (paired two-tailed Student's t test).

ophthalmic solution (Akorn), followed by gentle exposure of the eye globe. Intravitreal injection of 70 nL of a 150 μmol/L YK-4-279 (Cayman Chemicals #13661 or AdooQ #A11612) solution (reaching a final concentration of ∼10 μmol/L in an estimated vitreal volume of ∼1 μL) or vehicle (0.9% sterile saline) was performed using a Nanoject II (Drummond) nanoinjector. Eyelids were then reclosed around the eye, and erythromycin ophthalmic ointment (Akorn) was applied. Pups were warmed by hand until they regained consciousness and returned to their cages for 2 d.

Vasculogenic 3D Collagen Assays. HUVECs were purchased from Lonza and used from passages 3 to 6 as previously described (74, 75). HUVECs were suspended in 2.5 mg/mL collagen type I matrices, and assays were performed as described (74, 75), with the exception that the culture media contained reduced serum supplement, ascorbic acid, FGF-2, stem cell factor at 40 ng/mL, and interleukin-3 at 40 ng/mL. Stromal-derived factor-1α was added at 200 ng/mL into collagen type I matrices. Cultures were incubated at 37 °C in serum-free defined media and allowed to assemble over time. YK-4-279 was added to the cultures 48 h after tube formation at doses ranging from 20 to 0.15 μmol/L. The proinflammatory mediators, IL-1β (R&D Systems; #201-LB/CF) and TNFα (R&D Systems; #210-TA/CF), were added to cultures at different doses from 0 h, with or without YK-4-279. The lumen area was quantified using Metamorph software as previously described (74, 75). Individual data points were obtained from triplicate wells and a minimum of 12 independent fields from these wells. In some assays, triplicate wells were lysed with sample buffer, and Western blots were performed to probe for procaspase-3 (1:1,000, Cell Signaling; #9662S) and actin (1:500, Calbiochem; #CP01). Cultures were fixed at 72 h with 3% glutaraldehyde before staining with 0.1% toluidine blue in 30% methanol for nonfluorescent visualization.

Cell Culture under Sheer Stress. Flow-based cell culture was performed using HUVECs (ATCC; #PCS-100-010) cultured in complete EGM-2 media (Lonza). HUVECs were cultured on Ibidi Luer$^{0.6}$ flow slides and allowed to grow at 37 °C in 5% CO_2 for 24 h to a confluency of 80 to 90%. Slides were then attached to an Ibidi pump system with Perfusion Set Red (1.6 mm, #10962) and exposed to a sheer stress of 10 dyn/cm^2 for 24 h. Static conditions were achieved by similarly plating HUVECs in flow slides that were not exposed to flow. After 24 h of equilibration to flow conditions, cells were treated with 10 μmol/L YK-4-279 (or vehicle) for 24 h. Cells were gently washed with 1 mL ice-cold PBS and then fixed and permeabilized by incubation with ice-cold methanol for 5 min. Fixed cells were treated with 1% BSA and 0.02% Triton X-100 for 1 h at room temperature. Primary and secondary antibodies were added in 1% BSA and incubated for 2 h at room temperature.

Intravitreal Injection of YK-4-279 following Oxygen-Induced Retinopathy. Oxygen-induced retinopathy was performed using wild-type C57BL/6J mice as previously described (48, 49). Pups and their dams were maintained in room air from birth until P7.5. From P7.5 to P12.5, pups were exposed to 75% O_2 in an oxygen chamber regulated by an OxyCycler Model A84. After 2.5 d of oxygen exposure, the dams were replaced with healthy, lactating dams to prevent oxygen toxicity. At P12.5, pups were returned to room air until P17.5. At P17.5, pups were anesthetized by intraperitoneal injection of Ketamine (100 mg/kg body weight)/Xylazine (10 mg/kg body weight) and then given a 1-μL intravitreal injection of 40 μmol/L YK-4-279 (achieving a final concentration ∼10 μmol/L in an estimated vitreal volume of ∼4 μL) in one eye and a vehicle control in the contralateral eye. Mice were then returned to their cages for 2 d, at which time they were euthanized. Eye globes were fixed in 4% paraformaldehyde for 1 h at room temperature and then stored in PBS at 4 °C for <4 d. Retinas were immunostained for CD31, and blinded quantification of neovascularization was performed as previously described (48, 49).

Downloaded at Palestinian Territory, occupied on December 11, 2021

www.manaraa.com

Chromatin Immunoprecipitation. Chromatin Immunoprecipitation was performed as previously described (76) using HUVECs cultured in the presence of 10 μmol/L YK-4-279 (or a vehicle control) for 6 h. Following treatment, cells were fixed in culture flasks with 1% paraformaldehyde for 10 min at room temperature and quenched with 125 mmol/L glycine. Cells were washed with ice-cold PBS, scraped, and pelleted by centrifugation (350 × *g*, 5 min, 4 °C). Cells were then resuspended in 200 μL lysis buffer (1% sodium dodecyl sulfate [SDS], 10 mmol/L ethylenediaminetetraacetic acid [EDTA], 50 mmol/L Tris, pH 8.1, with added protease inhibitors) and incubated on ice for 15 min. Lysates were sonicated (five 20-s pulses at an amplitude of 45) using a Misonix S-4000 sonicator. Following sonication, 1.5 mL of dilution buffer (0.01% SDS, 1.1% Triton X-100, 1.2 mmol/L EDTA, 166.5 mmol/L NaCl, 16.7 mmol/L Tris, pH 8.1, with protease inhibitors) were added to each sample. Samples were then precleared using 60 μL protein A/G-conjugated agarose beads (Millipore) for 3 h at 4 °C with rotation. Beads were pelleted, and 10 μg anti-ERG (Abcam; #ab92513), anti-FLI1 (Abcam; #ab15289), anti-RNA Polymerase II (Abcam; #ab5408), or rabbit IgG (Millipore; #NI01) were added to the supernatants and rotated overnight at 4 °C.

Samples were then incubated with 60 μL protein A/G-conjugated agarose beads for 3 h at 4 °C with rotation. Antigen complexes were pelleted by centrifugation and washed two times with 1 mL low-salt buffer (0.1% SDS, 1% Triton X-100, 2 mmol/L EDTA, 150 mmol/L NaCl, 40 mmol/L Tris–HCl, pH 8.1), high-salt buffer (0.1% SDS, 1% Triton X-100, 2 mmol/L EDTA, 500 mmol/L NaCl, 40 mmol/L Tris–HCl, pH 8.1), LiCl buffer (1 mmol/L EDTA, 250 mmol/L LiCl, and 1% NaDeoxycholate), and TE buffer (1 mmol/L EDTA, 5 mmol/L Tris, pH 7.4), and rotated at 4 °C for 5 min. Samples were then incubated with 500 μL elution buffer (1% SDS, 100 mmol/L $NaHCO_3$) with rotation at room temperature for 45 min. Cross-links were reversed by incubated samples with 200 mmol/L NaCl at 65 °C overnight. DNA was purified by Proteinase K treatment (20 mg/mL), phenol-chloroform extraction, and ethanol precipitation. DNA was resuspended in ddH_2O and analyzed by qPCR using the primers 5′-CCAGCCCTCTGTGGAGAC-3′ and 5′-GCCTCCCCTTCAGGTTTTCC-3′, which flank a previously identified ERG regulatory site that lies within 200 bp upstream of the *Cdh5* transcriptional start site (38). Data are reported as the average of four to six technical replicates normalized to total input DNA from YK-4-279 and vehicle-treated samples.

Statistics. Prism 7.0 software (GraphPad Software) was used for all statistical assessments. Statistical comparisons made for in vivo studies (including Figs. 1*A* and *C*, 3*B*, and 5 *B* and *C*) used $n \geq 4$ biological replicates, and comparisons made for in vitro studies (including Figs. 3*D* and 4 *B* and *C*) used $n \geq 5$ technical replicates. Data normality was assessed using a Shapiro–Wilk test ($\alpha = 0.05$). Statistical significance between two groups was assessed by unpaired (Figs. 1*A*, 3*B*, and 4 *B* and *C*) and paired (Fig. 5 *B* and *C*) parametric two-tailed *t* tests. Comparison of multiples means (Figs. 1*C* and 3*D*) was made using repeated-measures ANOVA with multiple comparisons between individual group means. Statistically analyzed data are presented as mean ± SD.

Study Approval. Protocols involving mouse breeding and tamoxifen induction were approved by the Oklahoma Medical Research Foundation Institutional Animal Care and Use Committee. Protocols involving induction of OIR in mice were approved by the Oklahoma University Health Sciences Center Institutional Animal Care and Use Committee.

Data Availability. All study data are included in the article text and *SI Appendix*.

ACKNOWLEDGMENTS. We thank Jun Xie for mouse colony management and the C.T.G. laboratory members for helpful discussions. This work was supported by grants from the NIH (R35HL144605, P30GM114731, and P30EY021725); the Oklahoma Center for the Advancement of Science and Technology (HF18-014); and a grant from Research to Prevent Blindness (C5117328) awarded to the Department of Ophthalmology at the Dean McGee Eye Institute (University of Oklahoma Health Sciences Center).

1. Y. Sun, L. E. H. Smith, Retinal vasculature in development and diseases. *Annu. Rev. Vis. Sci.* **4**, 101–122 (2018).
2. P. A. Campochiaro, Ocular neovascularization. *J. Mol. Med. (Berl.)* **91**, 311–321 (2013).
3. P. K. Shah *et al.*, Retinopathy of prematurity: Past, present and future. *World J. Clin. Pediatr.* **5**, 35–46 (2016).
4. P. Lee, C. C. Wang, A. P. Adamis, Ocular neovascularization: An epidemiologic review. *Surv. Ophthalmol.* **43**, 245–269 (1998).
5. M. J. Kim, S. J. Kim, Y. S. Yu, The risk for retinal detachment associated with hemorrhages pre- and postlaser treatment in retinopathy of prematurity. *Retina* **28**, 1451–1457 (2008).
6. K. A. Hutcheson, A. T. Nguyen, M. W. Preslan, N. J. Ellish, S. M. Steidl, Vitreous hemorrhage in patients with high-risk retinopathy of prematurity. *Am. J. Ophthalmol.* **136**, 258–263 (2003).
7. E. M. Lad, T. Hernandez-Boussard, J. M. Morton, D. M. Moshfeghi, Incidence of retinopathy of prematurity in the United States: 1997 through 2005. *Am. J. Ophthalmol.* **148**, 451–458 (2009).
8. D. S. Fong *et al.*; American Diabetes Association, Retinopathy in diabetes. *Diabetes Care* **27** (suppl. 1), S84–S87 (2004).
9. H. Ozaki *et al.*, Blockade of vascular endothelial cell growth factor receptor signaling is sufficient to completely prevent retinal neovascularization. *Am. J. Pathol.* **156**, 697–707 (2000).
10. C. Pieh *et al.*, VEGF-A, VEGFR-1, VEGFR-2 and Tie2 levels in plasma of premature infants: Relationship to retinopathy of prematurity. *Br. J. Ophthalmol.* **92**, 689–693 (2008).
11. W. C. Wu *et al.*, An updated study of the use of bevacizumab in the treatment of patients with prethreshold retinopathy of prematurity in Taiwan. *Am. J. Ophthalmol.* **155**, 150–158.e1 (2013).
12. S. N. Chen *et al.*, Intravitreal anti-vascular endothelial growth factor treatment for retinopathy of prematurity: Comparison between ranibizumab and bevacizumab. *Retina* **35**, 667–674 (2015).
13. H. A. Mintz-Hittner, K. A. Kennedy, A. Z. Chuang; BEAT-ROP Cooperative Group, Efficacy of intravitreal bevacizumab for stage 3+ retinopathy of prematurity. *N. Engl. J. Med.* **364**, 603–615 (2011).
14. K. Kimoto, T. Kubota, Anti-VEGF agents for ocular angiogenesis and vascular permeability. *J. Ophthalmol.* **2012**, 852183 (2012).
15. R. S. Apte, D. S. Chen, N. Ferrara, VEGF in signaling and disease: Beyond discovery and development. *Cell* **176**, 1248–1264 (2019).
16. H. Wang, Anti-VEGF therapy in the management of retinopathy of prematurity: What we learn from representative animal models of oxygen-induced retinopathy. *Eye Brain* **8**, 81–90 (2016).
17. W. C. Wu *et al.*, Serum vascular endothelial growth factor after bevacizumab or ranibizumab treatment for retinopathy of prematurity. *Retina* **37**, 694–701 (2017).
18. J. Hu *et al.*, Reactivation of retinopathy of prematurity after bevacizumab injection. *Arch. Ophthalmol.* **130**, 1000–1006 (2012).
19. R. K. Wong, S. Hubschman, I. Tsui, Reactivation of retinopathy of prematurity after ranibizumab treatment. *Retina* **35**, 675–680 (2015).
20. D. Lepore *et al.*, Intravitreal bevacizumab versus laser treatment in type 1 retinopathy of prematurity: Report on fluorescein angiographic findings. *Ophthalmology* **121**, 2212–2219 (2014).
21. D. Lepore *et al.*, Follow-up to age 4 years of treatment of type 1 retinopathy of prematurity intravitreal bevacizumab injection versus laser: Fluorescein angiographic findings. *Ophthalmology* **125**, 218–226 (2018).
22. C. C. Tokunaga *et al.*, Effects of anti-VEGF treatment on the recovery of the developing retina following oxygen-induced retinopathy. *Invest. Ophthalmol. Vis. Sci.* **55**, 1884–1892 (2014).
23. M. Ito, M. Yoshioka, Regression of the hyaloid vessels and pupillary membrane of the mouse. *Anat. Embryol. (Berl.)* **200**, 403–411 (1999).
24. M. Silbert, A. S. Gurwood, Persistent hyperplastic primary vitreous. *Clin. Eye Vis. Care* **12**, 131–137 (2000).
25. R. A. Lang, J. M. Bishop, Macrophages are required for cell death and tissue remodeling in the developing mouse eye. *Cell* **74**, 453–462 (1993).
26. I. B. Lobov *et al.*, WNT7b mediates macrophage-induced programmed cell death in patterning of the vasculature. *Nature* **437**, 417–421 (2005).
27. G. Nayak *et al.*, Developmental vascular regression is regulated by a Wnt/β-catenin, MYC and CDKN1A pathway that controls cell proliferation and cell death. *Development* **145**, dev154898 (2018).
28. B. A. Parr, M. J. Shea, G. Vassileva, A. P. McMahon, Mouse Wnt genes exhibit discrete domains of expression in the early embryonic CNS and limb buds. *Development* **119**, 247–261 (1993).
29. J. M. Stenman *et al.*, Canonical Wnt signaling regulates organ-specific assembly and differentiation of CNS vasculature. *Science* **322**, 1247–1250 (2008).
30. W. Shu, Y. Q. Jiang, M. M. Lu, E. E. Morrisey, Wnt7b regulates mesenchymal proliferation and vascular development in the lung. *Development* **129**, 4831–4842 (2002).
31. Y. Yoshikawa *et al.*, Developmental regression of hyaloid vasculature is triggered by neurons. *J. Exp. Med.* **213**, 1175–1183 (2016).
32. A. Meeson, M. Palmer, M. Calfon, R. Lang, A relationship between apoptosis and flow during programmed capillary regression is revealed by vital analysis. *Development* **122**, 3929–3938 (1996).
33. S. F. Hackett, S. Wiegand, G. Yancopoulos, P. A. Campochiaro, Angiopoietin-2 plays an important role in retinal angiogenesis. *J. Cell. Physiol.* **192**, 182–187 (2002).
34. G. M. Koller *et al.*, Proinflammatory mediators, IL (Interleukin)-1β, TNF (tumor necrosis factor) α, and thrombin directly induce capillary tube regression. *Arterioscler. Thromb. Vasc. Biol.* **40**, 365–377 (2020).
35. M. Zhu *et al.*, The human hyaloid system: Cell death and vascular regression. *Exp. Eye Res.* **70**, 767–776 (2000).
36. A. P. Meeson, M. Argilla, K. Ko, L. Witte, R. A. Lang, VEGF deprivation-induced apoptosis is a component of programmed capillary regression. *Development* **126**, 1407–1415 (1999).
37. A. V. Shah, G. M. Birdsey, A. M. Randi, Regulation of endothelial homeostasis, vascular development and angiogenesis by the transcription factor ERG. *Vascul. Pharmacol.* **86**, 3–13 (2016).
38. G. M. Birdsey *et al.*, Transcription factor Erg regulates angiogenesis and endothelial apoptosis through VE-cadherin. *Blood* **111**, 3498–3506 (2008).

Downloaded at Palestinian Territory, occupied on December 11, 2021
www.manaraa.com

39. R. F. Gariano, T. W. Gardner, Retinal angiogenesis in development and disease. *Nature* **438**, 960–966 (2005).
40. S. Rahim *et al*., YK-4-279 inhibits ERG and ETV1 mediated prostate cancer cell invasion. *PLoS One* **6**, e19343 (2011).
41. B. Winters *et al*., Inhibition of ERG activity in patient-derived prostate cancer xenografts by YK-4-279. *Anticancer Res.* **37**, 3385–3396 (2017).
42. J. S. Barber-Rotenberg *et al*., Single enantiomer of YK-4-279 demonstrates specificity in targeting the oncogene EWS-FLI1. *Oncotarget* **3**, 172–182 (2012).
43. A. P. Looney *et al*., Synergistic role of endothelial ERG and FLI1 in mediating pulmonary vascular homeostasis. *Am. J. Respir. Cell Mol. Biol.* **57**, 121–131 (2017).
44. N. Nagai *et al*., Downregulation of ERG and FLI1 expression in endothelial cells triggers endothelial-to-mesenchymal transition. *PLoS Genet.* **14**, e1007826 (2018).
45. V. N. Pham *et al*., Combinatorial function of ETS transcription factors in the developing vasculature. *Dev. Biol.* **303**, 772–783 (2007).
46. C. Peghaire *et al*., The transcription factor ERG regulates a low shear stress-induced anti-thrombotic pathway in the microvasculature. *Nat. Commun.* **10**, 5014 (2019).
47. H. H. Lipowsky, Microvascular rheology and hemodynamics. *Microcirculation* **12**, 5–15 (2005).
48. K. M. Connor *et al*., Quantification of oxygen-induced retinopathy in the mouse: A model of vessel loss, vessel regrowth and pathological angiogenesis. *Nat. Protoc.* **4**, 1565–1573 (2009).
49. L. E. Smith *et al*., Oxygen-induced retinopathy in the mouse. *Invest. Ophthalmol. Vis. Sci.* **35**, 101–111 (1994).
50. M. V. Hoang, L. E. Smith, D. R. Senger, Calpain inhibitors reduce retinal hypoxia in ischemic retinopathy by improving neovascular architecture and functional perfusion. *Biochim. Biophys. Acta* **1812**, 549–557 (2011).
51. P. Hofman, B. C. van Blijswijk, P. J. Gaillard, G. F. Vrensen, R. O. Schlingemann, Endothelial cell hypertrophy induced by vascular endothelial growth factor in the retina: New insights into the pathogenesis of capillary nonperfusion. *Arch. Ophthalmol.* **119**, 861–866 (2001).
52. J. A. Montoya-Zegarra *et al*., AutoTube: A novel software for the automated morphometric analysis of vascular networks in tissues. *Angiogenesis* **22**, 223–236 (2019).
53. C. Korn, H. G. Augustin, Mechanisms of vessel pruning and regression. *Dev. Cell* **34**, 5–17 (2015).
54. N. Ricard, M. Simons, When it is better to regress: Dynamics of vascular pruning. *PLoS Biol.* **13**, e1002148 (2015).
55. C. A. Franco *et al*., Dynamic endothelial cell rearrangements drive developmental vessel regression. *PLoS Biol.* **13**, e1002125 (2015).
56. E. Kochhan *et al*., Blood flow changes coincide with cellular rearrangements during blood vessel pruning in zebrafish embryos. *PLoS One* **8**, e75060 (2013).
57. J. Plendl, Angiogenesis and vascular regression in the ovary. *Anat. Histol. Embryol.* **29**, 257–266 (2000).
58. S. Rao *et al*., Obligatory participation of macrophages in an angiopoietin 2-mediated cell death switch. *Development* **134**, 4449–4458 (2007).
59. V. Kalna *et al*., The transcription factor ERG regulates super-enhancers associated with an endothelial-specific gene expression program. *Circ. Res.* **124**, 1337–1349 (2019).
60. G. M. Birdsey *et al*., The endothelial transcription factor ERG promotes vascular stability and growth through Wnt/β-catenin signaling. *Dev. Cell* **32**, 82–96 (2015).
61. P. Paulo *et al*., FLI1 is a novel ETS transcription factor involved in gene fusions in prostate cancer. *Genes Chromosomes Cancer* **51**, 240–249 (2012).
62. J. P. Ginsberg *et al*., EWS-FLI1 and EWS-ERG gene fusions are associated with similar clinical phenotypes in Ewing's sarcoma. *J. Clin. Oncol.* **17**, 1809–1814 (1999).
63. H. V. Erkizan *et al*., A small molecule blocking oncogenic protein EWS-FLI1 interaction with RNA helicase A inhibits growth of Ewing's sarcoma. *Nat. Med.* **15**, 750–756 (2009).
64. S. Rahim *et al*., A small molecule inhibitor of ETV1, YK-4-279, prevents prostate cancer growth and metastasis in a mouse xenograft model. *PLoS One* **9**, e114260 (2014).
65. X. Wang *et al*., Development of peptidomimetic inhibitors of the ERG gene fusion product in prostate cancer. *Cancer Cell* **31**, 844–847 (2017).
66. M. S. Butler *et al*., Discovery and characterization of small molecules targeting the DNA-binding ETS domain of ERG in prostate cancer. *Oncotarget* **8**, 42438–42454 (2017).
67. S. M. Meadows, C. T. Myers, P. A. Krieg, Regulation of endothelial cell development by ETS transcription factors. *Semin. Cell Dev. Biol.* **22**, 976–984 (2011).
68. L. Yuan *et al*., ETS-related gene (ERG) controls endothelial cell permeability via transcriptional regulation of the claudin 5 (CLDN5) gene. *J. Biol. Chem.* **287**, 6582–6591 (2012).
69. L. Yuan *et al*., RhoJ is an endothelial cell-restricted Rho GTPase that mediates vascular morphogenesis and is regulated by the transcription factor ERG. *Blood* **118**, 1145–1153 (2011).
70. L. Yuan *et al*., Antiinflammatory effects of the ETS factor ERG in endothelial cells are mediated through transcriptional repression of the interleukin-8 gene. *Circ. Res.* **104**, 1049–1057 (2009).
71. Z. L. Grant *et al*., Blocking endothelial apoptosis revascularizes the retina in a model of ischemic retinopathy. *J. Clin. Invest.* **130**, 4235–4251 (2020).
72. Y. Wang *et al*., Ephrin-B2 controls VEGF-induced angiogenesis and lymphangiogenesis. *Nature* **465**, 483–486 (2010).
73. Y. Ohta *et al*., Articular cartilage endurance and resistance to osteoarthritic changes require transcription factor Erg. *Arthritis Rheumatol.* **67**, 2679–2690 (2015).
74. W. Koh, A. N. Stratman, A. Sacharidou, G. E. Davis, In vitro three dimensional collagen matrix models of endothelial lumen formation during vasculogenesis and angiogenesis. *Methods Enzymol.* **443**, 83–101 (2008).
75. A. N. Stratman, M. J. Davis, G. E. Davis, VEGF and FGF prime vascular tube morphogenesis and sprouting directed by hematopoietic stem cell cytokines. *Blood* **117**, 3709–3719 (2011).
76. M. T. Menendez, C. T. Griffin, Characterizing epigenetic changes in endothelial cells. *Methods Mol. Biol.* **1846**, 335–344 (2018).

Downloaded at Palestinian Territory, occupied on December 11, 2021

www.manaraa.com